Lee, K., McCray, W. H., Jr., & Doetsch, P. W. (1987) *Biochem. Biophys. Res. Commun. 149*, 93-101.
Radman, M (1976) *J. Biol. Chem. 251*, 1438-1445.
Teoule, R., Bonicel, A., Bert, C., Cadet, J., & Polverelli, M. (1974) *Radiat. Res. 57*, 46-58.
Wallace, S. S. (1988) *Environ. Mol. Mutagen. 12*, 431-477.
Weiss, R. B., & Duker, N. J. (1986) *Nucleic Acids Res. 14*, 6621-6631.
Weiss, R. B., & Duker, N. J. (1987) *Photochem. Photobiol. 45*, 763-768.

O^6-Ethylguanine Carcinogenic Lesions in DNA: An NMR Study of O^6etG·T Pairing in Dodecanucleotide Duplexes†

Matthew W. Kalnik,‡ Benjamin F. L. Li,§ Peter F. Swann,§ and Dinshaw J. Patel*,‡

Department of Biochemistry and Molecular Biophysics, College of Physicians and Surgeons, Columbia University, New York, New York 10032, and Biochemistry Department, University College London, London WC1E 6BT, England

Received January 20, 1989

ABSTRACT: High-resolution two-dimensional NMR studies are reported on the self-complementary d-(C1-G2-C3-O⁶etG4-A5-G6-C7-T8-T9-G10-C11-G12) duplex (designated O⁶etG·T 12-mer) containing two symmetrically related O⁶etG·T lesion sites located four base pairs in from either end of the duplex. Parallel studies were undertaken on a related sequence containing O⁶meG·T lesion sites (designated O⁶meG·T 12-mer) in order to evaluate the influence of the size of the alkyl substituent on the structure of the duplex and were undertaken on a related sequence containing G·T mismatch sites (designated G·T 12-mer duplex), which served as the control duplex. The exchangeable and nonexchangeable proton and the phosphorus nuclei have been assigned from an analysis of two-dimensional nuclear Overhauser enhancement (NOE) and correlated spectra of the O⁶etG·T 12-mer, O⁶meG·T 12-mer, and G·T 12-mer duplexes in H_2O and D_2O solutions. The distance connectivities observed in the NOESY spectra of the O⁶alkG·T 12-mer duplexes establish that the helix is right-handed and all of the bases adopt an anti conformation of the glycosidic torsion angle including the O⁶alkG4 and T9 bases at the lesion site. The imino proton of T9 at the O⁶alkG·T lesion sites resonates at 8.85 ppm in the O⁶etG·T 12-mer duplex and at 9.47 ppm in the O⁶meG·T 12-mer duplex. The large upfield shift of the T9 imino proton resonance at the O⁶alkG4·T9 lesion site relative to that of the same proton in the G4·T9 wobble pair (11.99 ppm) and the A4·T9 Watson–Crick pair (13.95 ppm) in related sequences establishes that the hydrogen bonding of the imino proton of T9 to O⁶alkG4 is either very weak or absent. The imino proton of T9 develops NOEs to the CH_3 protons of the O⁶etG and O⁶meG alkyl groups across the base pair, as well as to the imino and H5 protons of the flanking C3·G10 base pair and the imino and CH_3 protons of the flanking A5·T8 base pair in the O⁶alkG·T 12-mer duplexes. These observations establish that the O⁶alkG4 and T9 residues are stacked into the duplex and that the O^6CH_3 and $O^6CH_2CH_3$ groups of O⁶alkG4 adopt a syn orientation with respect to the N^1 of the alkylated guanine. The syn orientation of the O^6-alkyl group precludes wobble pairing at the O⁶alkG4·T9 lesion site and favors a Watson–Crick alignment of O⁶alkG4 and T9 stabilized by one short hydrogen bond between the 4-amino group of O⁶alkG4 and the 2-carbonyl oxygen of T9 in the minor groove. Since the O^6-alkyl group adopts a syn orientation, the separation between the O^6 of O⁶alkG4 and the O^4 of T9 in the major groove is increased, preventing the formation of a short hydrogen bond between the N^1 ring nitrogen of O⁶alkG4 and the imino proton of T9. Only small proton and phosphorus chemical shift differences were detected when the O⁶etG·T 12-mer and the O⁶meG·T 12-mer duplexes are compared, which reflect small conformational differences between the two duplexes. Much larger chemical shift differences are detected when the O⁶alkG·T 12-mer duplexes are compared with the G·T 12-mer duplex.

The mutagenic and carcinogenic action of *N*-nitroso compounds is in part due to the alkylation of the carbonyl groups of the purine and pyrimidine bases in DNA [reviewed by Pegg (1977), Singer (1979), and Singer and Grunberger (1983)]. The oxygen at position 6 of guanine is alkylated more often than the other exocyclic oxygen groups in DNA, and the formation of O^6-alkylguanine (O⁶alkG) is believed to play the most important role in *N*-nitrosamine carcinogenesis (Pegg, 1984). The alkylation of guanine in DNA leads to G·C → A·T transition mutations presumably by the mispairing of O⁶alkG with thymine (Loveless, 1969; Coulondre & Miller, 1977). A direct link between these mutations and the initiation of cancer has been suggested from animal studies (Pegg, 1984) and has been supported by the obervation that G·C → A·T transition mutations are the cause of the activation of the

†This research was supported by NIH GM 34504 to D.J.P. and grants from the Cancer Research Campaign and the Medical Research Council to P.F.S. NMR studies were conducted on instruments purchased with funds provided by the Robert Woods Johnson, Jr. Charitable Trust and the Matheson Foundation.

‡Columbia University.
§University College London.

0006-2960/89/0428-6170$01.50/0

Chart I

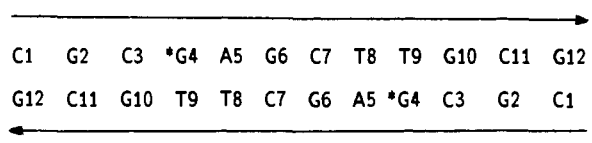

*G4 = G
= O^6meG
= O^6etG

H-ras-1 transforming gene during *N*-methyl-*N*-nitrosourea-induced mammary carcinogenesis (Sukumar et al., 1983; Zarbl et al., 1985).

The importance of the base-pairing properties of O⁶alkG has previously led us to conduct NMR studies of the structure of pairs between O⁶meG and C, T, A, and G located three base pairs in from either end of a self-complementary dodecanucleotide duplex (Patel et al., 1986a,b,c). From these studies, structures for base pairs involving O⁶meG were tentatively proposed. However, they did not define the orientation of the *O*⁶-methyl group. Additional evidence reported in this and the following paper (Kalnik et al., 1989) defines the orientation of the *O*⁶-methyl group, confirms the structure of the O⁶meG·T and O⁶meG·C (following paper) pairs previously proposed, and extends the investigation to the pairing of O⁶etG with T and C (following paper). The studies of the O⁶etG-containing oligomer were conducted to determine the structural effects of increasing size of the alkyl substituent, which might provide an explanation for the much slower metabolic repair of the *O*⁶-alkylguanines with long alkyl chains.

Three similar self-complementary dodecanucleotide duplexes (Chart I) with the general sequence d(C-G-C-*G-A-G-C-T-T-G-C-G), where *G is either guanine (designated G·T 12-mer), *O*⁶-methylguanine (designated O⁶meG·T 12-mer), or *O*⁶-ethylguanine (designated O⁶etG·T 12-mer), have been investigated in aqueous solution by two-dimensional proton and phosphorus NMR spectroscopy. The structural parameters deduced for the O⁶etG·T 12-mer duplex are compared with the corresponding parameters for the O⁶meG·T 12-mer duplex, and both of these duplexes are analyzed with reference to the control G·T 12-mer duplex, which has been reported previously (Kalnik et al., 1988).

Experimental Procedures

NMR Sample Preparation. Preliminary NMR investigations conducted on the O⁶alkG·T 12-mer duplexes at 0.1 M NaCl buffer concentrations indicated that the incorporation of the O⁶alkG destabilized the fully-paired duplex and a minor component (~5%, probably a hairpin) was observed. To shift the equilibrium toward the fully-paired duplex form, the NMR studies were undertaken in 1.1 M NaCl solution. The NMR spectra for the G·T 12-mer, O⁶meG·T 12-mer, and O⁶etG·T 12-mer duplexes were recorded in 1.1 M NaCl, 10 mM phosphate, and 1 mM EDTA aqueous buffer, henceforth called high-salt buffer. The concentration of each of the G·T 12-mer, O⁶meG·T 12-mer, and O⁶etG·T duplexes was ~400 A_{260} units in 0.40 mL. The pH values quoted in D_2O solution are uncorrected pH meter readings.

One-Dimensional NMR Experiments. All one-dimensional exchangeable proton NMR spectra were recorded with a sweep width of 20000 Hz, a 1–1 pulse (Hore et al., 1983) being used for water suppression with the carrier offset 6000 Hz downfield of the H_2O signal on a Bruker AM 500 spectrometer. The 121.5-MHz phosphorus spectra were collected on a Bruker AM 300 spectrometer with proton Waltz decoupling (Shaka et al., 1983) and a sweep width of 1000 Hz.

Two-Dimensional NMR Experiments. Phase-sensitive two-dimensional nuclear Overhauser effect (NOESY) spectra (Jeener et al., 1979; Macura et al., 1981) in H_2O solution were collected with quadrature detection, a repetition delay of 1.0 s, a sweep width of 10000 Hz with the carrier placed on the H_2O signal, and a mixing time of 120 ms. A jump–return solvent suppression pulse (Plateau & Gueron, 1982) was used for the detection pulse. The preparation and mixing pulses were reduced to 70° (~6.0 μs), diminishing the amount of transverse solvent magnetization at the end of the mixing period. This reduction allowed the jump–return acquisition pulse to achieve greater solvent suppression such that the receiver gain could be increased by at least a factor of 2, enhancing the sensitivity of the experiment. The waiting time between the jump and return pulses was optimized for even excitation of the imino, amino, and aromatic protons (65 μs). A total of 450 t_1 experiments were collected with 1024 complex data points and signal averaged for 256 scans. The real and imaginary data were collected nonsimultaneously and merged to yield 225 complex t_1 increments (States et al., 1982). The free induction decays were apodized with a 90°-shifted sine bell function to reduce truncation and 3-Hz line broadening to improve signal to noise in both dimensions. A fifth-order polynomial base-line correction was applied in both dimensions.

Phase-sensitive two-dimensional NOESY spectra in D_2O solution were collected with a repetition delay of 1.5 s, a sweep width of 5000 Hz, and a mixing time of 250 ms. The carrier frequency was positioned on the residual HOD resonance, which was suppressed with the decoupler channel. A total of 512 t_1 experiments were collected with 1024 complex data points in the t_2 dimension and 32 scans per t_1 experiment. Since the real and imaginary data points were acquired nonsimultaneously in the t_1 dimension, the 512 experiments were merged to yield 256 complex t_1 increments (States et al., 1982). The NOESY data sets were Fourier transformed in both dimensions with a 90°-shifted sine bell function zeroed to the 1024th point in the t_2 dimension and to the 256th point in the t_1 dimension.

Magnitude two-dimensional correlated (COSY) experiments (Aue et al., 1976; Nagayama et al., 1980) were recorded in D_2O solution with quadrature detection on a Bruker AM 500 spectrometer. A total of 512 t_1 increments were collected with a sweep width of 5000 Hz, 1024 complex data points in the t_2 dimension being used. The magnitude COSY data were collected with 32 scans per t_1 increment and a repetition delay of 1.5 s. The data sets were apodized with an unshifted sine bell function zeroed to the 512th point and Fourier transformed in both dimensions.

The phase-sensitive two-dimensional ^1H–^{31}P heteronuclear correlation experiments utilized an MLEV-17 composite pulse, which achieves a net exchange of magnetization between coupled protons via a homonuclear Hartmann–Hahn- (HOHAHA) type cross-polarization (Bax & Davis, 1985). This net magnetization transfer is then relayed to the ^{31}P atoms via an INEPT sequence (Zagorski & Norman, 1989). The carrier frequency was placed in the center of the 121.5-MHz phosphorus spectrum. The time domain data sets were accumulated over a sweep width of 300 Hz with 256 complex data points in the t_2 dimension. A sweep width of 2800 Hz was used in the t_1 dimension. Each t_1 increment was collected with a 1.0-s repetition delay and 1024 scans per increment. A total of 107 t_1 increments were collected for the G·T 12-mer duplex, 95 t_1 increments were collected for the O⁶meG·T

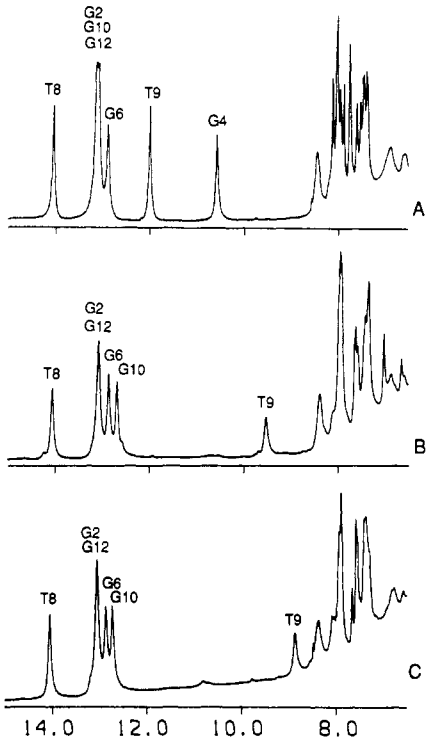

FIGURE 1: The 500-MHz proton NMR spectrum (6.5–15.0 ppm) of (A) the G·T 12-mer duplex, pH 6.2, (B) the O^6meG·T 12-mer duplex, pH 6.25, and (C) the O^6etG·T 12-mer duplex, 6.10, in 1.1 M NaCl, 10 mM phosphate, and H_2O at 15 °C.

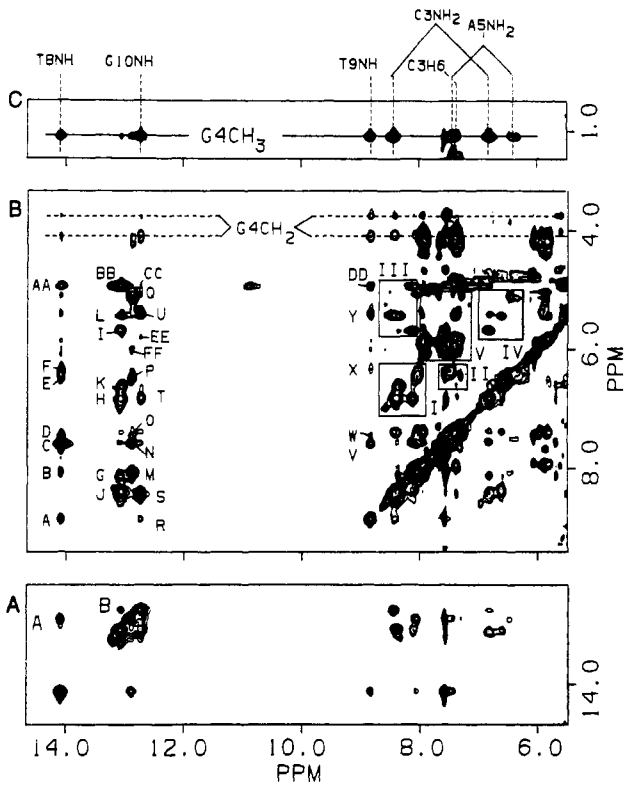

FIGURE 2: Phase-sensitive NOESY (120-ms mixing time) spectrum of the O^6etG·T 12-mer duplex in 1.1 M NaCl, 10 mM phosphate, and H_2O, pH 6.10 at 5 °C. (A) Cross-peaks establishing connectivities between imino protons in the symmetrical 12.0–14.5-ppm spectral range. (B) Cross-peaks establishing connectivities between the imino protons (5.0–14.5 ppm) and the base and amino protons (7.2–8.5 ppm). (C) Cross-peaks establishing connectivities between the CH_3 protons of the O^6-ethyl group of O^6etG4 (0.8–1.3 ppm) and the exchangeable imino and amino protons (5.0–14.5 ppm). Boxed regions I–V and cross-peaks A–Z are described in the text. Cross-peaks AA–DD represent chemical exchange cross-peaks between the exchangeable imino protons and the H_2O solvent protons. Cross-peaks EE and FF are weak cross-peaks involving guanine imino protons and cross-strand sugar H1′ protons.

12-mer duplex, and 104 t_1 increments were collected for the O^6etG·T 12-mer duplex. Both dimensions were zero filled to 1024 complex data points prior to Fourier transformation. The t_2 dimension was apodized with a Gaussian multiplication of −1.0 Hz and 0.04 broadening, and the t_1 dimension was apodized with a 90°-shifted sine bell function and 3-Hz exponential broadening.

Data Processing. The two-dimensional data sets were processed with FTNMR software (D. Hare, unpublished results) on a Vax 11-780 and a MicroVax II. The two-dimensional data sets were processed with the t_1 noise reduction routine of Otting et al. (1986) and symmetrized prior to plotting on either a Zeta 822 plotter or a Hewlett-Packard 7475a plotter for analysis, assignment, and publication figures.

Results

The numbering system of the parent G·T 12-mer, O^6meG·T 12-mer, and O^6etG·T 12-mer duplexes is outlined in Chart I.

Exchangeable Proton Spectra. Exchangeable proton NMR spectra (6.5–15.0 ppm) of the G·T 12-mer, O^6meG·T 12-mer, and O^6etG·T 12-mer duplexes in high-salt buffer–H_2O, pH ~6.2 at 15 °C, are presented in panels A–C of Figure 1, respectively. The spectra display similar patterns in the 12.5–14.2-ppm imino proton spectral region (Figure 1). The G·T 12-mer duplex exhibits five partially resolved imino protons corresponding to the single A·T and four G·C base pairs (Figure 1A). The guanine and thymine imino protons of the G4·T9 mismatch pair resonate at 10.52 and 11.99 ppm, respectively. The O^6meG·T 12-mer and O^6etG·T 12-mer duplexes exhibit five partially resolved imino protons for the single A·T and the four G·C base pairs (panels B and C of Figure 1, respectively). A sixth imino proton corresponding to the thymine imino of the O^6alkG4·T9 modification site resonates at 9.47 ppm in the O^6meG·T 12-mer duplex and at 8.85 ppm in the O^6etG·T 12-mer duplex, which is further upfield from its corresponding chemical shift (11.99 ppm) at the G4·T9 mismatch site within the G·T 12-mer duplex. The G4 imino proton is absent in the spectra of the O^6meG·T 12-mer and O^6etG·T 12-mer duplexes, since O^6-alkylation causes deprotonation at the N^1 position. All of the imino protons within the three duplexes have been assigned by analyzing the nuclear Overhauser enhancement (NOE) distance connectivities between exchangeable and nonexchangeable protons.

The phase-sensitive two-dimensional NOESY spectrum (120-ms mixing time) of the O^6etG·T 12-mer duplex in H_2O–high-salt buffer, pH 6.10 at 5 °C, is shown in Figure 2. The NOE cross-peaks between the imino (8.5–14.5 ppm) and aromatic/cytosine amino (5.0–9.0 ppm) protons are labeled as cross-peaks A–Y in Figure 2B. The most downfield imino proton displays a strong NOE to the H2 proton of A5 (peak C, Figure 2B) characteristic of Watson–Crick A·T base pairing, thereby establishing the assignment of the 14.05-ppm imino proton to residue T8. The four guanine imino protons of base pairs C1·G12, G2·C11, C3·G10, and G6·C7 also display intrabase pair NOEs to the hydrogen-bonded cytosine amino protons (peaks G, J, M, and S, respectively, Figure 2B) and to the exposed cytosine amino protons (peaks H, K, P, and T, respectively, Figure 2B) characteristic of Watson–Crick G·C base pairing. The guanine imino protons are assigned to specific positions in the sequence on the basis of NOEs to the flanking residues. The imino proton of G6 exhibits an NOE to the T8 imino proton (peak A, Figure 2A), and the

Table I: Proton Chemical Shifts in the O⁶etG·T 12-mer Duplex

	chemical shifts (ppm)[a]						
base pair	T-H3	G-H1	C-H4b	C-H4e	A-H6b	A-H6e	A-H2
C1·G12		13.04	8.09	6.84			
G2·C11		13.04	8.38	6.59			
C3·G10		12.70	8.43	6.79			
O⁶etG4·T9	8.85						
A5·T8	14.05				7.48	6.31	7.59
G6·C7		12.86	8.09	6.45			

	chemical shifts (ppm)[b]								
base	H8	H2	H6	H5/CH3	H1′	H2′	H2″	H3′	H4′
C1			7.63	5.84	5.75	1.98	2.43	4.73	4.11
G2	8.00				5.98	2.70	2.82	5.04	4.42
C3			7.41	5.49	5.52	2.02	2.36	4.88	4.23
O⁶etG4	8.02				5.87	2.73	2.90	5.08	4.43
A5	7.97	7.68			5.99	2.62	2.81	5.08	4.43
G6	7.72				5.89	2.60	2.71	5.00	4.48
C7			7.38	5.20	6.03	2.12	2.59	4.83	4.32
T8			7.50	1.63	6.16	2.25	2.58	4.96	4.24
T9			7.47	1.81	5.91	2.23	2.53	4.96	4.28
G10	7.99				5.89	2.72	2.72	5.07	4.48
C11			7.44	5.51	5.89	1.98	2.40	4.90	4.27
G12	7.96				6.17	2.46	2.69	4.76	

[a] 1.1 M NaCl, 10 mM phosphate, H_2O, pH 6.10, 5 °C; exchangeable protons. [b] 1.1 M NaCl, 10 mM phosphate, D_2O, pH 6.0, 25 °C; nonexchangeable protons.

imino proton of G10 exhibits NOEs to the imino protons of G2 (peak B, Figure 2A) and T9 (peak R, Figure 2B). Several other NOEs are observed between adjacent base pairs and within the same base pair, providing further confidence in the above assignments: The 14.05-ppm imino proton of T8 develops NOEs to the imino proton of T9 (peak A, Figure 2B) and to the hydrogen-bonded and exposed amino protons of C7 (peaks B and E, Figure 2B, respectively) and A5 (peaks D and F, Figure 2B). The imino protons of G12 (13.04 ppm), G2 (13.04 ppm), G6 (12.86 ppm), and G10 (12.70 ppm) all exhibit NOEs to their respective intrabase pair H5 proton of residues C1, C11, C7, and C3 (peaks I, L, Q, and U, Figure 2B, respectively). The 12.86-ppm imino proton of G6 also exhibits NOEs to the hydrogen-bonded and exposed amino protons of the adjacent A5 residue (peaks O and P, Figure 2B). The assignment of the 8.85-ppm imino proton of T9 is based on the NOEs observed to the two flanking imino protons of T8 (peak A, Figure 2B) and G10 (peak R, Figure 2B), to the H2 and hydrogen-bonded and exposed amino protons of A5 (peaks V, W, and X, Figure 2B, respectively), and to the H5 proton of residue C3 (peak Y, Figure 2B). NOEs are also observed between the hydrogen-bonded and exposed amino protons of cytosine (box I, Figure 2B) and of adenine (box II, Figure 2B), between the hydrogen-bonded amino protons and the H5 protons of cytosine within the same base pair (box III, Figure 2B), and between the exposed amino protons and the H5 protons of cytosine within the same base pair (box IV, Figure 2B). The nonexchangeable base proton to sugar H1′ NOE connectivities (see next section) can be traced in this NOESY spectrum in H_2O if box V of Figure 2B is expanded. The chemical shift assignments of the exchangeable imino and amino protons and the nonexchangeable adenine H2 protons of the O⁶etG·T 12-mer in high-salt buffer, pH 6.10 and 5 °C, are listed in the upper part of Table I. Each of the imino protons also develops chemical exchange cross-peaks with the solvent H_2O of varying intensity (peaks AA–DD, Figure 2B).

The 1.13-ppm CH_3 protons of residue O⁶etG4 develop NOEs to several exchangeable protons in the phase-sensitive NOESY experiment in H_2O–high-salt buffer, pH 6.10 at 5 °C (see line, Figure 2C). These include the imino protons of T8, T9, and G10 and the hydrogen-bonded and exposed amino protons of C3 and A5 (Figure 2C). The 3.85-ppm CH_2 proton of O⁶etG4 develops weaker NOEs to exchangeable protons, which include the imino protons of T8, T9, and G10 and the hydrogen-bonded amino protons of C3 (see pair of dashed lines in Figure 2B). The remaining cross-peaks have been identified as NOEs involving nonexchangeable sugar H5′,5″ protons of the terminal C1 residue which resonate coincidently with the 3.85-ppm CH_2 proton of O⁶etG4.

Almost identical cross-peak patterns are observed in the phase-sensitive NOESY spectrum (120-ms mixing time) of the O⁶meG·T 12-mer duplex in H_2O–high-salt buffer, pH 6.25 at 5 °C (Figure 3). The cross-peaks are readily assigned, and the correspnding chemical shifts are listed at the top of Table II. The cross-peak labels A–Z and boxed regions I–V identify the same cross-peaks within the NOESY spectra of the O⁶meG·T 12-mer (Figure 3) and the O⁶etG·T 12-mer (Figure 2) duplexes. The most significant difference is that the thymine imino proton of O⁶alkG4·T9 resonates at 8.85 ppm in the O⁶etG·T 12-mer duplex and at 9.47 ppm in the O⁶meG·T 12-mer duplex. Other small differences include the absence of the NOE between the imino proton of T9 and the exposed amino proton of A5 (peak X) in the O⁶meG·T 12-mer duplex and the increased intensity of two weak tentatively assigned NOEs between the imino protons of G6 and the sugar H1′ proton of C7 (peak FF) and between the imino proton of G10 and the sugar H1′ proton of C11 (peak EE) in the O⁶meG·T 12-mer duplex. The chemical shift assignments of the exchangeable imino and amino protons and nonexchangeable adenine H2 protons of the O⁶meG·T 12-mer in high-salt buffer, pH 6.25 at 5 °C, are listed in the upper part of Table II.

The OCH_3 group of O⁶meG4 was specifically labeled with 90% ^{13}C at the O^6CH_3 position in the O⁶meG·T 12-mer duplex. The ^{13}C–^1H scalar coupling splits the $O^{13}CH_3$ protons into a doublet resonating at 3.56 and 3.86 ppm. A third resonance at 3.71 ppm is also observed corresponding to the 10% of unlabeled O^6CH_3 groups. The $O^{13}CH_3$ protons develop several strong NOEs to neighboring exchangeable protons in the phase-sensitive NOESY spectrum in H_2O of the O⁶meG·T 12-mer duplex (see pair of solid lines, Figure 3C). The $O^{13}CH_3$ protons exhibit NOEs to the imino protons of T8, T9, and G10 and to the hydrogen-bonded amino protons of C3 and A5 and to the exposed amino protons of C3 (Figure 3C).

Table II: Proton Chemical Shifts in the O^6meG·T 12-mer Duplex

	chemical shifts (ppm)[a]						
base pair	T-H3	G-H1	C-H4b	C-H4e	A-H6b	A-H6e	A-H2
C1·G12		13.07	8.13	6.89			
G2·C11		13.04	8.39	6.60			
C3·G10		12.64	8.38	6.65			
O^6meG4·T9	9.47						
A5·T8	14.06				7.48	6.20	7.58
G6·C7		12.83	8.01	6.48			

	chemical shifts (ppm)[b]								
base	H8	H2	H6	H5/CH3	H1′	H2′	H2″	H3′	H4′
C1			7.59	5.81	5.72	1.94	2.40	4.69	4.08
G2	7.97				5.93	2.67	2.78	5.00	4.39
C3			7.35	5.44	5.62	1.98	2.37	4.85	4.19
O^6meG4	7.98				5.77	2.67	2.83	5.03	4.38
A5	7.95	7.64			5.99	2.59	2.81	5.04	4.44
G6	7.65				5.80	2.54	2.65	4.97	4.43
C7			7.35	5.17	5.95	2.08	2.53	4.75	4.19
T8			7.46	1.59	6.12	2.19	2.57	4.91	4.23
T9			7.42	1.75	5.83	2.23	2.49	4.90	4.19
G10	7.92				5.87	2.66	2.71	5.02	4.39
C11			7.37	5.45	5.82	1.94	2.35	4.86	4.20
G12	7.92				6.13	2.41	2.65	4.71	

[a] 1.1 M NaCl, 10 mM phosphate, H_2O, pH 6.25, 5 °C; exchangeable protons. [b] 1.0 M NaCl, 10 mM phosphate, D_2O, pH 6.35, 25 °C; nonexchangeable protons.

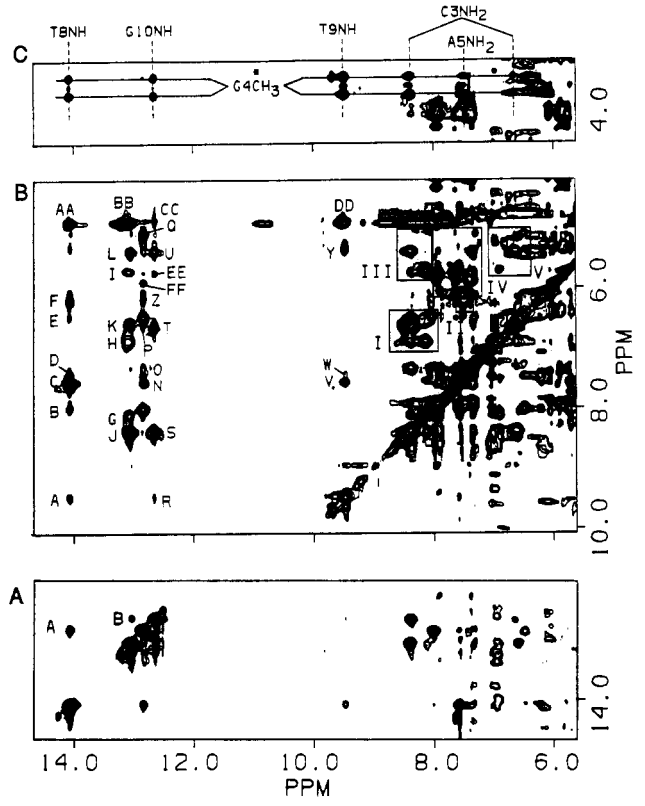

FIGURE 3: Phase-sensitive NOESY (120-ms mixing time) spectrum of the O^6meG·T 12-mer duplex in 1.1 M NaCl, 10 mM phosphate, and H_2O, pH 6.25 at 5 °C. (A) Cross-peaks establishing connectivities between imino protons in the symmetrical 12.0–14.5-ppm spectral range. (B) Cross-peaks establishing connectivities between the imino protons (5.0–14.5 ppm) and the base and amino protons (7.2–8.5 ppm). (C) Cross-peaks establishing connectivities between the O^6CH_3 protons of O^6meG4 (3.5–4.5 ppm) and the exchangeable imino and amino protons (5.0–14.5 ppm). Boxed regions I–V and cross-peaks A–Z are described in the text. Cross-peaks AA–DD represent chemical exchange cross-peaks between the exchangeable imino protons and the H_2O solvent protons. Cross-peaks EE and FF are weak cross-peaks involving guanine imino protons and cross-strand sugar H1′ protons.

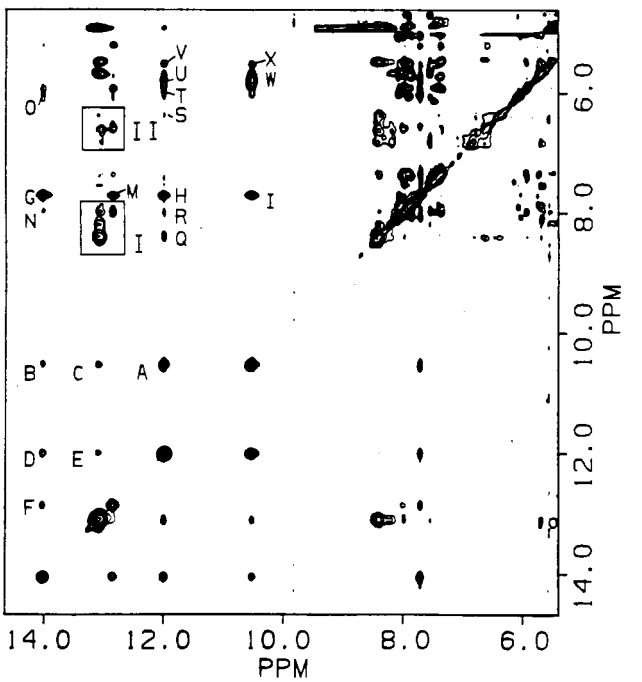

FIGURE 4: Phase-sensitive NOESY (120-ms mixing time) spectrum of the G·T 12-mer duplex in 1.1 M NaCl, 10 mM phosphate, and H_2O, pH 6.2 at 5 °C. Cross-peaks A–M have been assigned in the magnitude NOESY spectrum at 10 °C in H_2O reported previously (Kalnik et al., 1988). Cross-peaks N–X and boxes I and II are described in the text.

Expanded contour plots of the phase-sensitive two-dimensional NOESY spectrum (120-ms mixing time) of the G·T 12-mer duplex in H_2O–high-salt buffer, pH 6.2 at 5 °C, are given in Figure 4. The adenine amino protons, the exposed amino protons of cytosine, and the amino protons of residue G4 at the G4·T9 mismatch site are observed in the phase-sensitive spectrum at 5 °C, which were not originally observed in the previously reported magnitude NOESY spectrum at 10 °C (Kalnik et al., 1988). The additional NOEs observed in Figure 4 are labeled N–X and are assigned as follows: The hydrogen-bonded and exposed amino protons of A5 (7.97 and 6.03 ppm, respectively) develop NOEs to the 14.03-ppm imino proton of T8 (peaks N and O, Figure 4) and to the 11.99-ppm imino proton of T9 (Peaks R and T, Figure 4). The two amino protons of G4 resonate coincidently at 5.78 ppm and display

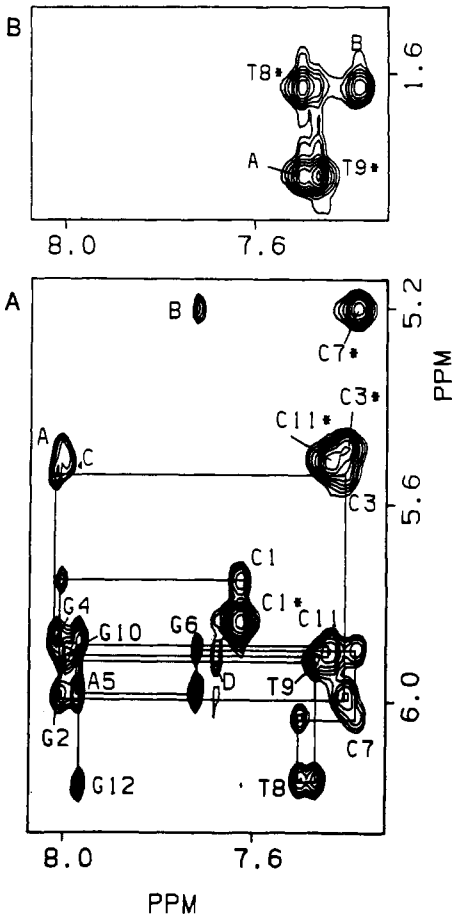

FIGURE 5: Expanded contour plots of the phase-sensitive NOESY spectrum (mixing time 250 ms) of the O⁶etG·T 12-mer duplex in 1.1 M NaCl, 10 mM phosphate, and D_2O, pH 6.00 at 25 °C. (A) Distance connectivities between the base protons (7.0–8.5 ppm) and the sugar H1′ protons (5.0–6.4 ppm). (B) Distance connectivities between the base protons (7.0–8.5 ppm) and the CH_3 protons (1.5–1.9 ppm). The cytosine H6–H5 and thymine H6–$CH_3$5 cross-peaks are designated by asterisks. The cross-peaks A–D are discussed in the text. The lines follow connectivities between adjacent base protons and their intervening sugar H1′ protons in the O⁶etG·T 12-mer duplex.

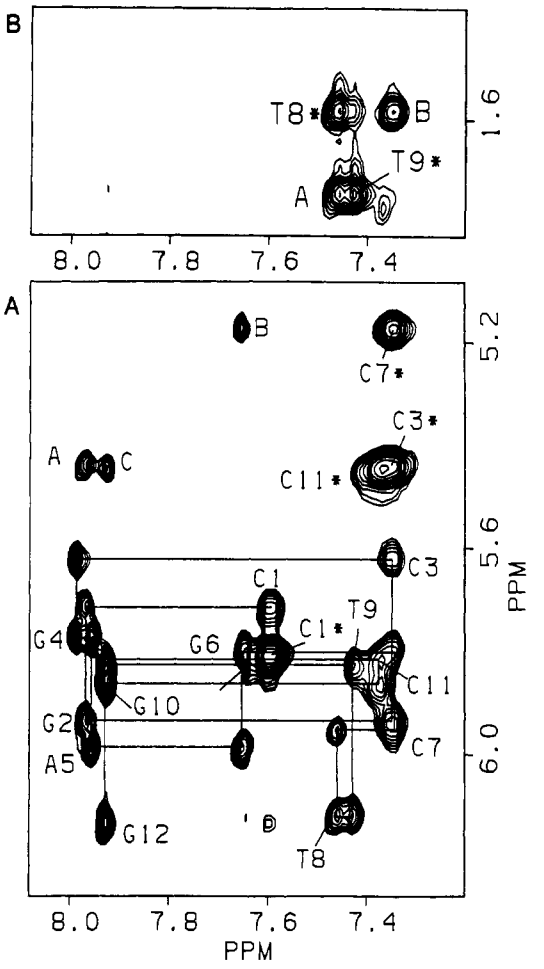

FIGURE 6: Expanded contour plots of the phase-sensitive NOESY spectrum (mixing time 250 ms) of the O⁶meG·T 12-mer duplex in 1.1 M NaCl, 10 mM phosphate, and D_2O, pH 6.35 at 25 °C. (A) Distance connectivities between the base protons (7.0–8.5 ppm) and the sugar H1′ protons (5.0–6.4 ppm). (B) Distance connectivities between the base protons (7.0–8.5 ppm) and the CH_3 protons (1.5–2.0 ppm). The cytosine H6–H5 and thymine H6–$CH_3$5 cross-peaks are designated by asterisks. The cross-peaks A–C are discussed in the text. The lines follow connectivities between adjacent base protons and their intervening sugar H1′ protons in the O⁶meG·T 12-mer duplex.

NOEs to the imino protons of T9 (peak U, Figure 4) and G4 (peak W, Figure 4). The characteristic NOEs observed between the imino protons of guanine and the hydrogen-bonded and exposed amino protons of cytosine in Watson–Crick base pairs are observed for the four G·C pairs in the G·T 12-mer duplex (boxes I and II). Several other distance connectivities are observed involving the imino protons at the mismatch site and include the NOEs between the imino proton of T9 and the H5 (peak V, Figure 4) and hydrogen-bonded (peak Q, Figure 4) and exposed (peak S, Figure 4) amino protons of C3 and between the imino proton of G4 and the H5 proton of C3 (peak X, Figure 4). The exchangeable imino and amino and nonexchangeable adenine H2 proton assignments for the G·T 12-mer duplex in high-salt buffer, pH 6.2 at 5 °C, are given in the upper part of Table III.

Nonexchangeable Proton Spectra. The nonexchangeable base and sugar protons in regular DNA oligonucleotide duplexes can be assigned on the basis of through-space distance connectivities in two-dimensional NOESY data sets [reviewed by Reid (1987), Patel et al. (1987), and Van de Ven and Hilbers (1988)]. Expanded regions of the phase-sensitive NOESY spectrum of the O⁶etG·T 12-mer duplex and the O⁶meG·T 12-mer duplex in D_2O–high-salt buffer at 25 °C are plotted in Figures 5 and 6, respectively. In the O⁶etG·T 12-mer duplex, the base protons resonate between 7.3 and 8.1 ppm, the sugar H1′ and cytosine H5 protons resonate between 5.1 and 6.4 ppm, and the thymine CH_3 protons resonate between 1.6 and 1.9 ppm. The strong cross-peaks between the H5 and H6 protons of the four cytosines and between the CH_3-5 and H6 protons of the two thymines are designated by asterisks in Figure 5. The purine H8 and pyrimidine H6 base protons exhibit NOEs to their own and 5′-linked sugar protons along the entire length of the O⁶etG·T 12-mer duplex (Hare et al., 1983; Scheek et al., 1984; Weiss et al., 1984). The NOE connectivities can be followed from residue C1 to residue G12 including the O⁶etG4·T9 modification site and are traced in Figure 5A. Potential ambiguities in the tracing were resolved by analyzing distance connectivities in the rest of the NOESY spectrum. NOEs are also observed between base protons on adjacent residues within the same strand at the purine H8/pyrimidine H6(3′–5′)pyrimidine H5/CH_3 steps at G2-C3 (peak A, Figure 5A), G6-C7 (peak B, Figure 5A), C7-T8 (peak B, Figure 5B), T8-T9 (peak A, Figure 5B), and G10-C11 (peak C, Figure 5A). Furthermore, an interstrand NOE is observed between the H2 proton of A5 and the H1′ proton of T9 (peak D, Figure 5A). A similar strategy has been used to assign the sugar H2′, H2″, H3′, and H4′ protons in the O⁶etG·T 12-mer duplex at 25 °C, which have been confirmed

Table III: Proton Chemical Shifts in the G·T 12-mer Duplex

	chemical shifts (ppm)[a]							
base pair	T-H3	G-H1	C-H4b	C-H4e	A-H6b	A-H6e	A-H2	G-H2b,e
C1·G12		13.08	8.20	6.79				
G2·C11		13.08	8.41	6.59				
C3·G10		13.08	8.40	6.37				
G4·T9	11.99	10.52						5.78
A5·T8	14.03				7.97	6.03	7.71	
G6·C7		12.85	7.98	6.58				

	chemical shifts (ppm)[b]								
base	H8	H2	H6	H5/CH3	H1′	H2′	H2″	H3′	H4′
C1			7.61	5.82	5.74	1.94	2.43	4.75	
G2	8.01				5.96	2.75	2.83	5.06	4.44
C3			7.45	5.55	5.81	2.17	2.51	4.91	4.25
G4	7.86				5.71	2.63	2.86	5.07	4.42
A5	8.10	7.75			6.07	2.65	2.95	5.10	4.47
G6	7.72				5.79	2.58	2.68	5.04	4.46
C7			7.39	5.26	5.96	2.07	2.56	4.80	4.28
T8			7.46	1.62	6.18	2.14	2.65	4.94	4.28
T9			7.51	1.86	5.60	2.26	2.39	4.94	4.11
G10	8.02				5.99	2.76	2.80	5.08	4.45
C11			7.37	5.51	5.80	1.94	2.36	4.88	4.21
G12	7.94				6.15	2.46	2.69		

[a] 1.1 M NaCl, 10 mM phosphate, H_2O, pH 6.2, 5 °C; exchangeable protons. [b] 1.1 M NaCl, 10 mM phosphate, D_2O, pH 6.2, 25 °C; nonexchangeable protons.

by an analysis of the COSY spectrum under the same experimental conditions. The nonexchangeable base and sugar proton chemical shift assignments for the O⁶etG·T 12-mer in high-salt buffer, pH 6.0 at 25 °C, are listed in the lower part of Table I.

The proton resonances of the OCH_2CH_3 group of O⁶etG4 resonate at 1.16 ppm (CH_3 protons) and 4.12 and 3.85 ppm (nonequivalent CH_2 protons) in the O⁶etG·T 12-mer duplex. One-dimensional slices through the CH_3 and CH_2 protons of residue O⁶etG4 in the NOESY spectrum of the O⁶etG·T 12-mer duplex, D_2O at 25 °C, are plotted in panels A and B of Figure 7, respectively. Strong NOEs are observed from the CH_3 protons to the two nonequivalent CH_2 protons within the O⁶etG4 residue, as well as to the H5 proton of C3 of the C3·G10 base pair in one direction and the CH_3 group of T8 of the A5·T8 base pair in the other direction (Figure 7A). Much weaker NOEs are detected from the CH_3 protons of O⁶etG4 to the H6 proton of C3 and to the CH_3 protons of T9 in the O⁶etG·T 12-mer duplex (Figure 7A). The corresponding one-dimensional slice taken through the 3.85-ppm CH_2 proton resonance of residue O⁶etG4 displays two strong NOEs, one to the other CH_2 proton at 4.11 ppm and one to the CH_3 protons within the O⁶etG4 residue (Figure 7B). Several other weaker NOEs are observed but are difficult to unambiguously assign since the 3.85-ppm CH_2 proton of O⁶etG4 resonates at the same frequency as the H5′,5″ protons of C1 (Figure 7B).

Expanded contour plots of the phase-sensitive (mixing time 250 ms) NOESY spectrum of the O⁶meG·T 12-mer duplex in D_2O–high-salt buffer, pH 6.35 at 25 °C, are shown in Figure 6. The tracing of the base proton to sugar proton NOE connectivities is straightforward, as outlined in Figure 6A. The nonexchangeable base and sugar H1′, H2′, H2″, H3′, and H4′ protons have been assigned in the O⁶meG·T 12-mer duplex, and these chemical shifts are listed in the lower part of Table II.

A one-dimensional slice through the 3.86-ppm $O^{13}CH_3$ proton resonance of O⁶meG4 in the NOESY spectrum in D_2O shows strong NOEs to the H5 proton of C3 and to the CH_3 protons of T8 (Figure 7C).

The nonexchangeable base and sugar protons in the G·T 12-mer duplex in high-salt buffer have been assigned previously

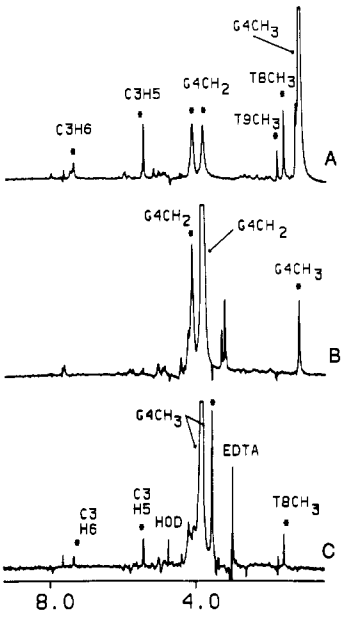

FIGURE 7: One-dimensional slices taken through (A) the CH_3 protons of O⁶etG4 and (B) one of the nonequivalent CH_2 protons of O⁶etG4 in the phase-sensitive NOESY spectrum (250-ms mixing time) of the O⁶etG·T 12-mer duplex in 1.1 M NaCl, 10 mM phosphate, and D_2O, pH 6.0 at 25 °C. (C) A slice taken through the CH_3 protons of O⁶meG4 in the phase-sensitive NOESY spectrum (250-ms mixing time) of the O⁶meG·T 12-mer duplex in 1.1 M NaCl, 10 mM phosphate, and D_2O, pH 6.35 at 25 °C. NOEs are designated by asterisks.

(Kalnik et al., 1988) and are listed in the lower part of Table III.

Phosphorus Spectra. The 121.5-MHz proton Waltz decoupled phosphorus spectra of the G·T 12-mer, O⁶meG·T 12-mer, and O⁶etG·T 12-mer are plotted in panels A–C of Figure 8, respectively. The phosphorus resonances in all three duplexes were assigned by recording and analyzing heteronuclear ^1H–^{31}P COSY spectra (Zagorski & Norman, 1989) as described below for the O⁶etG·T 12-mer duplex (Figure 9A). Each phosphorus has the potential to develop direct and relayed couplings to the H3′, H4′, H1′, and H2′,2″ protons of the O3′-linked sugar and to the H4′ and H5′,5″ protons of the O5′-linked sugar on the basis of the conformationally

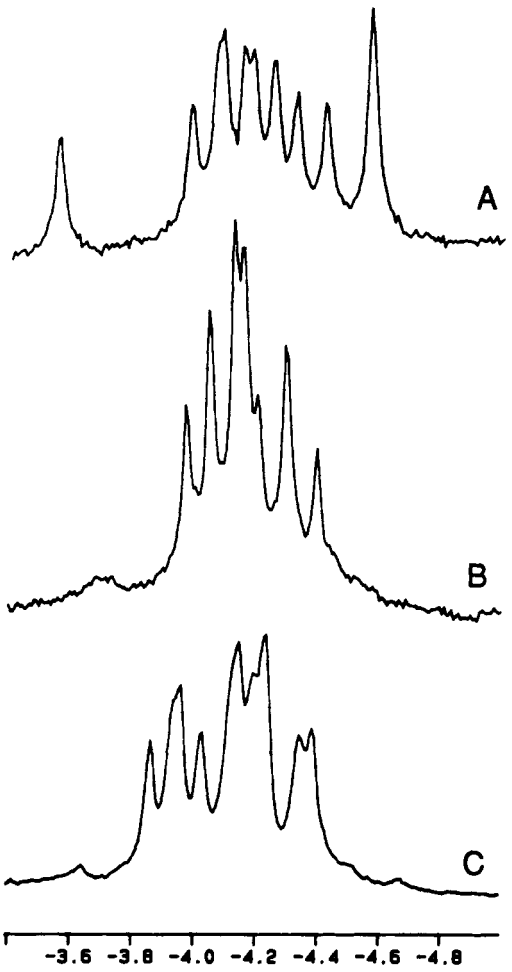

FIGURE 8: Proton Waltz decoupled 121.5-MHz phosphorus spectra (−3.0 to −5.5 ppm) of (A) the G·T 12-mer duplex, pH 6.25, (B) the O⁶meG·T 12-mer duplex, pH 6.35, and (C) the O⁶etG·T 12-mer duplex, pH 6.00, in 1.1 M NaCl, 10 mM phosphate, and D_2O at 25 °C.

Table IV: ^{31}P–^{1}H Heteronuclear Correlations and ^{31}P Chemical Shifts in the O⁶etG·T, O⁶meG·T,[a] and G·T[a] 12-mer Duplexes at 25 °C

	chemical shifts (ppm)				
	P	H3′[b]	H4′[b]	H2′,2″[b]	H4′[c]
O⁶etG·T 12-mer					
C3-O⁶etG4	−3.86	4.90	4.24	2.04, 2.38	4.45
O⁶etG4-A5	−4.23	5.10	4.48		4.48
T8-T9	−4.24	4.95			4.27
T9-G10	−4.16	4.97	4.25	2.23, 2.51	4.45
O⁶meG·T 12-mer					
C3-O⁶meG4	−4.00	4.86	4.21	1.95, 2.38	4.40
O⁶meG4-A5	−4.19	5.04	4.43		4.43
T8-T9	−4.31	4.90			4.19
T9-G10	−4.14	4.91		2.23, 2.45	4.40
G·T 12-mer					
C3-G4	−4.07	4.91	4.25	2.17, 2.50	4.42
G4-A5	−4.58	5.07	4.43		4.49
T8-T9	−4.57	4.95			4.11
T9-G10	−3.54	4.94	4.15	2.27, 2.37	4.47

[a] Data not shown. [b] O3′-Linked ^{31}P–^{1}H correlations. [c] O5′-Linked ^{31}P–^{1}H correlations.

dependent strength of the individual couplings. Every phosphorus was assigned through the scalar coupling connectivities to the sugar H3′ protons, and any ambiguities were resolved by analyzing the relay cross-peaks to the H2′,2″ and the H4′ protons. This is demonstrated in the slice through the most downfield (assigned to C3-O⁶etG4) resonance at −3.86 ppm as shown in Figure 9B. The phosphorus resonance assignments

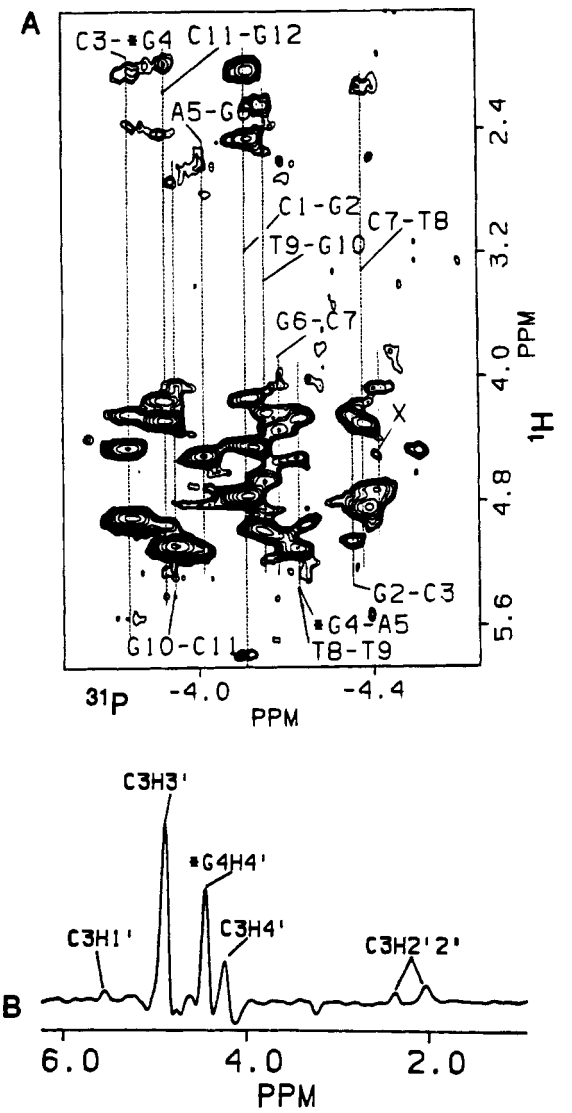

FIGURE 9: (A) Two-dimensional heteronuclear phosphorus (observe)–proton COSY contour plot of the O⁶etG·T 12-mer duplex, D_2O solution at 25 °C. Note that only the positive contour levels are plotted for clarity, and the reference is to the positive contours. (B) A one-dimensional slice taken through the most downfield phosphorus resonance (−3.86 ppm) corresponding to the C3-O⁶etG4 phosphodiester group in the proton–phosphorus COSY in (A). Heteronuclear correlations to the O3′- and O5′-linked sugar protons are designated above each resonance. Cross-peak X is not assignable to any of the phosphodiester groups in the major form of the O⁶etG·T 12-mer duplex and may be due to the minor component in the sample (presumably hairpin).

Table V: ^{31}P Chemical Shifts in the O⁶etG·T 12-mer, O⁶meG·T 12-mer, and the G·T 12-mer Duplexes at 25 °C[a]

	chemical shifts (ppm)		
P	O⁶etG·T	O⁶meG·T	G·T
C1-G2	−4.12	−4.14	−4.06
G2-C3	−4.35	−4.31	−4.15
C3-*G4	−3.86	−4.00	−4.07
*G4-A5	−4.23	−4.19	−4.57
A5-G6	−4.02	−4.05	−4.32
G6-C7	−4.20	−4.14	−4.17
C7-T8	−4.39	−4.40	−4.41
T8-T9	−4.24	−4.31	−4.58
T9-G10	−4.16	−4.14	−3.54
G10-C11	−3.96	−4.05	−4.24
C11-G12	−3.93	−4.00	−3.97

[a] 1.1 M NaCl, 10 mM phosphate, pH ~6.2, D_2O.

and the observed ^{1}H–^{31}P scalar coupling connectivities within the (C3-*G4-A5)·(T8-T9-G10) segment centered about the

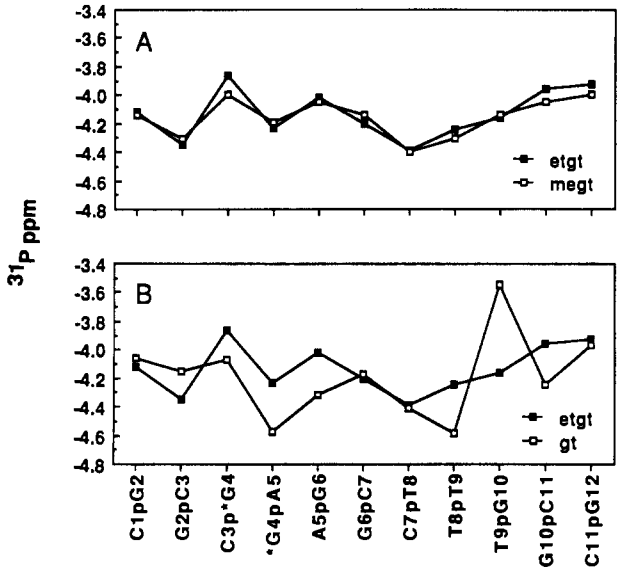

FIGURE 10: Graphical comparison of ^{31}P chemical shift as a function of phosphodiester position between (A) the O^{6}etG·T 12-mer duplex and the O^{6}meG·T 12-mer duplex and (B) the O^{6}etG·T 12-mer duplex and the G·T 12-mer duplex.

lesion site in all three duplexes are given in Table IV. The phosphorus chemical shift assignments for phosphodiester backbone groups along the entire length of the helix in the G·T 12-mer, O^{6}meG·T 12-mer, and O^{6}etG·T 12-mer duplexes are listed in Table V.

The phosphorus resonances of the O^{6}meG·T 12-mer (Figure 8B) and the O^{6}etG·T 12-mer (Figure 8C) duplexes exhibit similar chemical shifts (Figure 10A) except for the C3-O^{6}alkG4 step where the −3.86 ppm resonance in the O^{6}etG·T 12-mer duplex is shifted downfield of its −4.00 ppm counterpart in the O^{6}meG·T 12-mer duplex.

The phosphorus spectrum of the G·T 12-mer duplex (Figure 8A) displays resonances at −3.54 (T9-G10), −4.57 (T8-T9), and −4.58 ppm (G4-A5) which are outside the chemical shift range (−4.0 to −4.5 ppm) for unperturbed phosphodiester resonances in right-handed DNA. Significant chemical shift differences are detected between the phosphates in the O^{6}etG·T 12-mer and the G·T 12-mer duplexes (Figure 10B), and these differences extend beyond the (C3-*G4-A5)·(T8-T9-G10) segment centered about the lesion site.

Discussion

The pairing of O^{6}etG and O^{6}meG with thymine in self-complementary deoxynucleotide duplexes has been probed by analyzing the distance and coupling connectivities in two-dimensional NMR experiments.

General Structure of DNA Duplexes. The NMR spectra show that the duplexes containing G·T, O^{6}meG·T, and O^{6}etG·T base pairs form right-handed double helices, with every nucleoside including the alkylated nucleoside having the normal anti glycosidic torsion angle and with every base pair except the alkylated and G·T pairs having the normal Watson–Crick configuration.

The base to sugar proton distance connectivities observed for right-handed DNA are intact at the modification site in all three duplexes, indicating that G·T [see Kalnik et al. (1988)], O^{6}meG·T (Figure 6A), and O^{6}etG·T (Figure 5A) base pairs are accommodated into a right-handed helix. The observation of directional base proton to base proton NOEs at purine(3′–5′)pyrimidine steps and directional NOEs between the minor groove adenine H2 protons and sugar H1′ protons [Figures 6 and 7; see also Kalnik et al. (1988)] indicate that all three helices are right-handed over their entire length (Hare et al., 1983; Scheek et al., 1984; Weiss et al., 1984).

The conformation of the glycosidic torsion angle, syn or anti, can be determined by monitoring the NOE between the purine H8 or pyrimidine H6 proton and its own sugar H1′ proton (Patel et al., 1982) and by comparing its intensity to the intensity of the fixed interproton distance NOE of the cytosine H5–H6 interaction (~2.4 Å). In the syn conformation, the base proton to sugar H1′ interproton distance is ~2.4 Å, and in the anti conformation the same interproton distance is ~3.7 Å. When the glycosidic torsion angle assumes the syn conformation, the intensity of the base proton to sugar H1′ proton NOE is similar to the intensity of the fixed-distance cytosine H5–H6 NOE. In the anti conformation, the base proton to sugar H1′ proton NOE is much weaker than the cytosine H5–H6 NOE. Every NOE observed between base protons and their own sugar H1′ protons is much weaker than the NOEs observed between the H5 and H6 cytosine protons within the same base, indicating that every residue in all three duplexes maintains an anti conformation of the glycosidic torsion angle.

The presence of Watson–Crick base pairs can be established from the chemical shift of the imino protons and the presence of characteristic NOE distance connectivities. The hydrogen-bonded imino protons characteristically resonate between 12.0 and 14.5 ppm. The five unmodified base pairs in each symmetrical half of the G·T 12-mer, O^{6}meG·T 12-mer, and O^{6}etG·T 12-mer duplexes all have an imino proton resonating between 12.0 and 14.5 ppm (Figure 1), indicating that the base pairs are intact. In addition, the thymine imino protons of the A·T base pairs display intrabase pair NOEs to the adenine H2 protons, which is characteristic of Watson–Crick base pairing, and the guanine imino protons of the unmodified G·C base pairs display intrabase pair NOEs to the cytosine amino protons, also characteristic of Watson–Crick pairing (Figures 2–4). The G4 imino and T9 imino protons of the mismatch base pair in the G·T 12-mer duplex are each shifted approximately 2.0 ppm upfield of their Watson–Crick imino proton counterparts, since the hydrogen-bond acceptor for these wobble imino protons is a carbonyl oxygen rather than a ring nitrogen as in Watson–Crick base pairs. The T9 imino protons of the O^{6}meG4·T9 base pair and of the O^{6}etG4·T9 base pair in their respective duplexes are shifted between 4.0 and 5.0 ppm upfield from the Watson–Crick imino proton chemical shift region. This extremely large upfield chemical shift establishes that the hydrogen bonding of the imino protons of T9 to O^{6}alkG4 is either very weak or absent.

The results discussed immediately above would suggest that these helices are, in broad terms, similar to B-form DNA. An insight into the extent of the deviation from this normal structure can be gained from the ^{31}P spectra. The ^{31}P spectrum of the G·T 12-mer duplex (Figure 8A) indicates that incorporation of a wobble G·T base pair into a right-handed DNA helix perturbs the phosphodiester backbone sufficiently such that three phosphorus resonances are shifted outside of the normal chemical shift range of phosphodiester groups in regular right-handed DNA (−3.9 to −4.4 ppm). These shifted phosphorus resonances correspond to the T9-G10 (−3.54 ppm), G4-A5 (−4.58 ppm), and T8-T9 (−4.57 ppm) phosphodiesters in the (C3-G4-A5)·(T8-T9-G10) segment at the mismatch site.

By contrast, the ^{31}P spectra for the O^{6}meG·T 12-mer duplex (Figure 8B) has all of its narrow resonances falling in the −3.9- to −4.4-ppm range, suggesting that the phosphodiester backbone has a relatively unperturbed conformation and that the

Table VI: Nonexchangeable Proton Chemical Shift Differences between the O⁶etG·T 12-mer Duplex and the O⁶meG·T 12-mer and the G·T 12-mer Duplexes[a]

	Δδ (ppm)	
	O⁶etG·T/O⁶meG·T	O⁶etG·T/G·T
C3·G10		
G-H8	−0.07	0.03
C-H6	−0.06	0.04
C-H5	−0.05	0.06
G-H′	−0.02	0.10
C-H1′	0.10	0.28
*G4·T9		
G-H8	−0.04	−0.16
T-H6	−0.05	0.04
T-CH3	−0.06	0.05
G-H1′	−0.12	−0.18
T-H1′	−0.08	−0.31
A5·T8		
A-H8	−0.02	0.13
A-H2	−0.04	0.07
T-H6	−0.04	−0.04
T-CH3	−0.04	−0.01
A-H1′	0.00	0.08
T-H1′	−0.04	0.02

[a] 1.1 M NaCl, 10 mM phosphate, D_2O. The pH of the G·T 12-mer duplex was 6.25, the pH of the O⁶meG·T 12-mer duplex was 6.35, and the pH of the O⁶etG·T 12-mer duplex was 6.00.

O⁶meG4·T9 base pair is readily incorporated into the helix with minimal distortion. The perturbation is larger in the case of the O⁶etG·T 12-mer duplex (Figure 8C) since the C3-O⁶etG4 phosphate resonates at −3.86 ppm, which is downfield of the −3.9- to −4.4-ppm region. The respective phosphodiester resonance assignments of the O⁶meG·T 12-mer and O⁶etG·T 12-mer duplexes are similar except for changes at the C3-O⁶etG4 phosphodiester linkage reflecting distortions introduced by the bulkier *O*⁶-ethyl adduct (Figure 10A). The similarity between the conformation of the O⁶meG·T 12-mer and the O⁶etG·T 12-mer in the (C3-O⁶alkG4-A5)·(T8-T9-G10) segment is confirmed by the spectrum of the nonexchangeable protons. Only two protons in this segment have chemical shift differences that are 0.10 ppm or greater between the O⁶etG·T 12-mer and the O⁶meG·T 12-mer duplexes (Table VI). The H1′ proton of C3 experiences a 0.10-ppm downfield shift and the H1′ proton of O⁶alkG4 proton experiences a 0.12-ppm upfield shift when proceeding from the O⁶etG·T 12-mer to the O⁶meG·T 12-mer duplex. These small chemical shift differences may reflect small changes in the glycosidic torsion angles at the C3 and O⁶alkG4 residues as the size of the alkyl adduct is increased.

Several weak broad resonances are observed to low and high field of the main cluster of resonances in the phosphorus spectra of O⁶meG·T 12-mer and O⁶etG·T 12-mer. These resonances may be due to the minor component (presumably a hairpin) that has been observed in the proton spectra.

Structure of the O⁶alkG·T Base Pair. The stacking of the O⁶etG4 and T9 bases into the helix has been confirmed by the observation of many interbase pair NOEs in the (C3-O⁶etG4-A5)·(T8-T9-G10) segment. The glycosidic torsion angles of both the O⁶etG4 and T9 residues in the O⁶etG·T 12-mer duplex are in the anti range since the H8 proton to its sugar H1′ proton NOE observed for O⁶etG4 and the H6 proton to sugar H1′ proton NOE observed for T9 are much weaker than any of the NOEs observed between the H5 and H6 protons within each cytosine (Figure 5A).

Determining the orientation of the *O*⁶-alkyl group is critical for elucidation of the pairing alignment of the O⁶alkG base with thymine. The CH_3 of the *O*⁶-methyl group and the CH_2 of the *O*⁶-ethyl group can be in either an anti conformation (Chart IIA) or a syn conformation (Chart IIB) with respect to the N^1 position of guanine.

Chart II

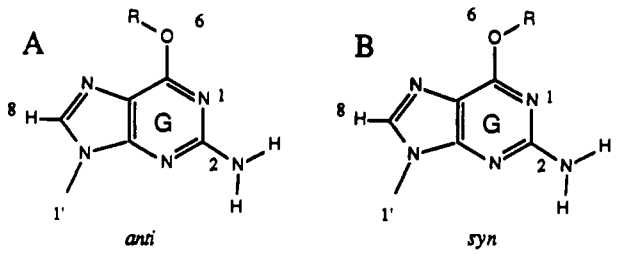

Chart III

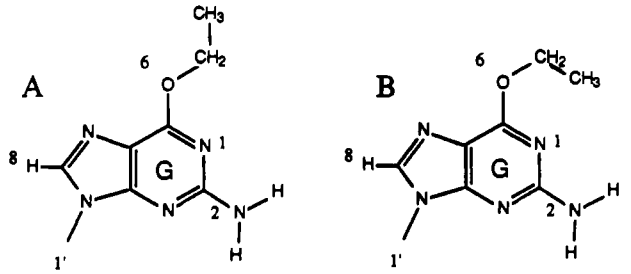

The CH_3 protons of O⁶etG4 in the O⁶etG·T 12-mer duplex display NOEs to the following protons: the CH_2 protons of the *O*⁶-ethyl group of O⁶etG4, the major groove H5, H6, and amino protons of the 5′-flanking C3 residue, the major groove adenine amino protons of the 3′-flanking A5 residue, the major groove CH_3 protons of the flanking T8 residue on the opposite strand, the major groove CH_3 protons of the T9 residue, and the imino protons of T8, T9, and G10 (Figures 2 and 7A). The CH_2 protons of O⁶etG4 display NOEs to the following protons: the CH_3 protons of O⁶etG4, the hydrogen-bonding amino proton of C3, and the imino protons of T8, T9, and G10 (Figures 2 and 7B). The distance connectivities detected between the CH_3 and the CH_2 protons of O⁶etG4 and the imino proton of T9 establish a syn orientation (Chart IIB) and rule out an anti orientation (Chart IIA) of the $O^6CH_2CH_3$ group at the O⁶etG4·T9 modification site in the O⁶etG·T 12-mer duplex.

The NOE connectivities involving the *O*⁶-methyl protons of O⁶meG4 in the O⁶meG·T 12-mer duplex are similar to those for the C_2H_5 protons of O⁶etG4. The $O^{13}CH_3$ protons of O⁶meG4 develop NOEs to the following protons: the H5, H6, and amino protons of C3, the hydrogen-bonded amino proton of A5, the CH_3 protons of T8, and the imino protons of T8, T9, and G10 (Figures 3 and 7C). The strongest NOE observed involving the CH_3 protons of O⁶meG4 is to the imino proton of T9, placing the CH_3 protons in a syn orientation (Chart IIB).

For a given orientation of the CH_2 of the *O*⁶-ethyl group, the CH_3 has some freedom of movement. The extremes of its possible conformations are depicted in Chart III. If the proposed O⁶etG·T base pair is modeled in a B-DNA helix, it can be seen that the CH_3 group of O⁶etG4 would be closer to the H5 of adjacent C3 if the ethyl group adopts the orientation outlined in Chart IIIA, while the CH_3 group of O⁶etG4 would be closer to the imino proton of T9 across the base pair if the ethyl group adopts the orientation outlined in Chart IIIB. Since sizable NOEs are detected from the CH_3 protons of O⁶etG4 to both the H5 of C3 (Figure 7A) and the imino proton of T9 (Figure 2C), the observed distance connectivities do not permit an unambiguous differentiation between the orientations of the CH_3 group about the CH_2–CH_3

Chart IV

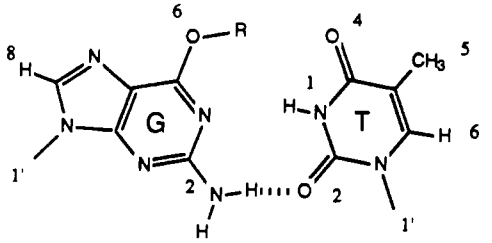

bond of O^{6}etG4 (Chart III). Indeed, the data are consistent with the CH_3 protons in a rapid equilibrium between the two orientations depicted in Chart III.

The possibility of hydrogen bonding in the O^{6}etG4·T9 base pair is very dependent on the orientation of the *O*^{6}-ethyl group. The results discussed above establish that the *O*^{6}-ethyl group of O^{6}etG4 is oriented toward T9 with the alkyl group acting as a spacer between the O^6 of O^{6}etG4 and the O^4 of T9 across the major groove of the O^{6}etG4·T9 pair. This spreading apart of the O^{6}etG4·T9 base pair in the major groove (Chart IV) is also reflected in the anomalous chemical shift (8.85 ppm) of the imino proton of T9, which indicates that the T9 imino proton is not involved in a hydrogen bond with the N^1 of O^{6}etG4. Further evidence supporting the absence of a hydrogen bond between the N^1 of O^{6}etG4 and the imino proton of T9 is that the imino proton of T9 exchanges more rapidly with solvent (peak DD, Figure 2B) than any of the other nonterminal imino protons within the O^{6}etG·T 12-mer duplex.

These results support a Watson–Crick alignment of the O^{6}etG4·T9 base pair in the O^{6}etG·T 12-mer duplex with the O^{6}etG4 and T9 bases spread apart along the major groove, preventing the imino proton of T9 from hydrogen bonding to the N^1 of O^{6}etG4 and allowing only one hydrogen bond to form between the 2-amino group of O^{6}etG4 and the O^2 of T9, on the basis of their proximity in the proposed model (Chart IV).

The proposed pairing of the O^{6}meG4·T9 base pair in the O^{6}meG·T 12-mer duplex is given in Chart IV. Similar arguments as given above for the O^{6}etG·T base pair can be made for the O^{6}meG·T base pair. Since the O$^6CH_3$ protons of O^{6}meG4 are in a syn conformation, they act as a spacer between the O^6 of O^{6}meG4 and the O^4 of T9, causing the bases to be spread apart on the major groove side of the O^{6}meG4·T9 base pair. However, the 0.54-ppm downfield shift of the T9 imino proton, from 8.85 ppm in the O^{6}etG·T 12-mer duplex to 9.47 ppm in the O^{6}meG·T 12-mer duplex, suggests that the T9 imino proton changes from not being involved in a hydrogen bond in the O^{6}etG4·T9 base pair to possibly being involved in a weak hydrogen bond in the O^{6}meG4·T9 base pair. The loss of hydrogen bonding of the imino proton of T9 due to the increasing size of the alkyl substituent in the O^{6}alkG4·T9 base pair can be rationalized by the orientation of the CH_2CH_3 group of O^{6}etG4 shown in Chart IIIB, which would increase the spacing between the O^6 of O^{6}alkG4 and the O^4 of T9 in the O^{6}etG4·T9 base pair relative to that in the O^{6}meG4·T9 base pair.

Comparison of O^{6}etG·T and G·T Base Pairing. The proposed Watson–Crick alignment for the O^{6}etG4·T9 lesion pair (Chart IV) and the wobble alignment for the G4·T9 mismatch pair (Chart V) should be reflected in chemical shift differences between the O^{6}alkG·T and G·T 12-mer duplexes among the base and sugar protons centered about the modification site. Experimentally, these differences in base-pair overlap are reflected in chemical shift differences at the imino proton of

Chart V

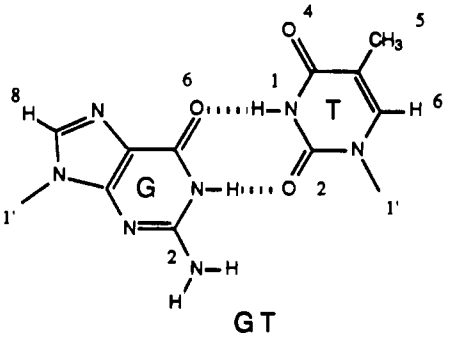

G3, the H8 proton of *G4, and the H8 proton of A5, while changes in glycosidic torsion angles are reflected in chemical shift differences at the H1′ proton of C3, *G4, and T9 between the O^{6}etG·T 12-mer and the G·T 12-mer duplexes (Table VI).

The 3.1-ppm upfield shift of the T9 imino proton from 11.99 ppm in the G·T 12-mer duplex to 8.85 ppm in the O^{6}etG·T 12-mer duplex must reflect a change from a hydrogen-bonded N^3 imino proton of T9 with the O^6 carbonyl of G4 at the G4·T9 mismatch site (Chart V) to a non-hydrogen-bonded imino proton of T9 at the O^{6}etG4·T9 lesion site (Chart IV).

The spectral dispersion of the phosphorus resonances is much larger in the G·T 12-mer duplex (Figure 8A) than in the O^{6}etG·T 12-mer duplex (Figure 8B). These results indicate a greater perturbation of the phosphodiester backbone upon insertion of a wobble G·T mismatch pair than upon insertion of an O^{6}etG·T lesion pair, which maintains a Watson–Crick alignment. The largest chemical shift difference is detected at the T9-C10 step (Figure 10B). Other significant differences are also detected along the length of the helix except for the terminal C1-G2 and C11-G12 steps and the central G6·C7 and C7-T8 steps (Figure 10B).

These significant differences in base pair overlap, glycosidic torsion angles, sugar puckers, and backbone conformation between the O^{6}etG·T base pair and the G·T base pair embedded in otherwise identical duplexes further substantiate the conclusion that the O^{6}etG4 and T9 residues of the O^{6}etG·T base pair are not aligned in a wobble manner.

Comparison with Earlier Studies. A previous NMR study reported on O^{6}meG·T lesions incorporated three base pairs in from either end of a self-complementary dodecanucleotide duplex (Patel et al., 1986b). This study did not address the question of syn versus anti orientations of the *O*^{6}-methyl group, although it also concluded that the O^{6}meG and T bases were aligned in a Watston–Crick manner stabilized by a single hydrogen bond in the minor groove.

To date, molecular mechanics calculations of O^{6}meG·T pairing are based solely on anti orientations of the O$^6CH_3$ group with the pairing at the lesion site stabilized by hydrogen bonding with the lone pair electrons of the O$^6CH_3$ group (Caldwell & Kollman, 1985). The present experimental demonstration of a syn orientation of the *O*^{6}-alkyl group precludes participation of the O^6 atom in hydrogen-bond formation. Hence, the computations should be repeated with the *O*^{6}-alkyl group in a syn orientation to define the pairing at the O^{6}alkG·T lesion site in DNA duplexes.

Conclusions. These NMR studies have demonstrated that the O^{6}alkG·T lesions are readily incorporated into DNA helices. The bases at the lesion site adopt an anti conformation of the glycosidic torsion angle, stack with the flanking Watson–Crick base pairs, and introduce localized conformational perturbations of the helix. The O^{6}alkG·T lesion pair maintains a Watson–Crick alignment of the bases with one strong and

possibly one weak hydrogen bond in the case of O^{6}meG·T. The NMR parameters demonstrate that the *O*^{6}-alkyl group adopts a syn orientation for the O^{6}alkG·T lesions. The *O*^{6}-alkyl group in a syn orientation projects toward the base on the partner strand and restricts the possible pairing alignments at the lesion site. The alkyl group acts as a spacer between the guanine O^6 and thymine O^4 atoms with a resulting increase in the separation between the guanine N^1 and thymine N^3 atoms at the lesion site (Chart IV).

The base-pairing properties of guanine is greatly affected by alkylation at the O^6-position. The N^1 imino proton is lost upon alkylation, and the bulky nature of the alkyl moiety prevents close contact of the bases in the major groove. This steric hindrance introduced by alkylation in the major groove is alleviated in the O^{6}alkG·T base pairs by a spreading of the bases while a Watson–Crick alignment is retained stabilized by a single strong hydrogen bond. NMR studies on O^{6}alkG·C lesions (Kalnik et al., 1989) indicate that the unfavorable steric interactions between the *O*^{6}-alkyl group and the 4-NH_2 protons of cytosine are relieved through wobble pairing stabilized by two hydrogen bonds. The possible biological implications of these results are discussed at greater length in the following paper. These studies suggest that other structural features such as the alignment of the bases at the active site of the DNA polymerase during replication are responsible for the preferential pairing of O^{6}alkG with T observed in vitro and in vivo, rather than the number of hydrogen bonds stabilizing the pairing interaction. A similar conclusion has been reached by Strazewski (1988) from studies on deazacytosine in DNA.

Registry No. G·T 12-mer, 111616-39-8; O^{6}meG·T 12-mer, 121157-91-3; O^{6}etG·T 12-mer, 121157-92-4.

References

Aue, W. P., Bartholdi, E. E., & Ernst, R. R. (1976) *J. Chem. Phys. 64*, 2229–2246.

Bax, A., & Davis, D. G. (1985) *J. Magn. Reson. 65*, 355–360.

Caldwell, J. W., & Kollman, P. A. (1985) *J. Biomol. Struct. Dyn. 3*, 57–66.

Coulondre, C., & Miller, J. H. (1977) *J. Mol. Biol. 117*, 577–606.

Hare, D. R., Wemmer, D. E., Chou, S. H., Drobny, G., & Reid, B. R. (1983) *J. Mol. Biol. 171*, 319–336.

Hore, P. J. (1983) *J. Magn. Reson. 55*, 283–300.

Jeener, J., Meier, B. H., Bachman, P., & Ernst, R. R. (1979) *J. Chem. Phys. 71*, 4546–4553.

Kalnik, M. W., Kouchakdjian, M., Li, B. F. L., Swann, P. F., & Patel, D. J. (1988) *Biochemistry 27*, 108–115.

Kalnik, M. W., Li, B. F. L., Swann, P. F., & Patel, D. J. (1989) *Biochemistry* (following paper in this issue).

Loveless, A. (1969) *Nature 223*, 206–208.

Macura, S., Huang, Y., Suter, D., & Ernst, R. R. (1980) *J. Magn. Reson. 40*, 321–334.

Nagayama, K., Kumar, A., Wuhtrich, K., & Ernst, R. R. (1980) *J. Magn. Reson. 40*, 321–334.

Otting, G., Widmer, H., Wagner, G., & Wuhtrich, K. (1986) *J. Magn. Reson. 66*, 187–193.

Patel, D. J., Kozlowski, S. A., Nordheim, A., & Rich, A. (1982) *Proc. Natl. Acad. Sci. U.S.A. 79*, 1413–1417.

Patel, D. J., Shapiro, L., Kozolowski, S. A., Gaffney, B. L., & Jones, R. A. (1986a) *Biochemistry 25*, 1027–1036.

Patel, D. J., Shapiro, L., Kozolowski, S. A., Gaffney, B. L., & Jones, R. A. (1986b) *Biochemistry 25*, 1036–1042.

Patel, D. J., Shapiro, L., Kozolowski, S. A., Gaffney, B. L., & Jones, R. A. (1986c) *J. Mol. Biol. 188*, 677–692.

Patel, D. J., Shapiro, L., & Hare, D. R. (1987) *Q. Rev. Biophys. 20*, 35.

Pegg, A. E. (1977) *Adv. Cancer Res. 25*, 195–269.

Pegg, A. E., & Singer, B. (1984) *Cancer Invest. 2*, 221–238.

Plateau, P., & Gueron, M. (1982) *J. Am. Chem. Soc. 104*, 7310–7311.

Reid, B. R. (1987) *Q. Rev. Biophys. 20*, 1–34.

Scheek, R. M., Boelens, R., Russo, N., van Boom, J. H., & Kaptein, R. (1984) *Biochemistry 23*, 1371–1376.

Shaka, A. J., Keeler, J., Frenkiel, T., & Freeman, R. (1983) *J. Magn. Reson. 52*, 335–338.

Singer, B. (1979) *J. Natl. Cancer Inst. 62*, 1329–1339.

Singer, B., & Grunberger, D. (1983) in *Molecular Biology of Mutagens and Carcinogens*, Plenum, New York.

States, D. J., Haberkorn, R. A., & Reuben, D. J. (1982) *J. Magn. Reson. 48*, 286–292.

Strazewski, P. (1988) *Nucleic Acids Res. 16*, 9377–9399.

Sukumar, S., Notario, V., Martin-Zanca, D., & Barbacid, M. (1983) *Nature 306*, 658–662.

Van de Ven, F., & Hilbers, C. W. (1988) *Eur. J. Biochem. 178*, 1–38.

Weiss, M. A., Patel, D. J., Sauer, R. T., & Karplus, M. (1984) *Proc. Natl. Acad. Sci. U.S.A. 81*, 130–134.

Zagorski, M. G., & Norman, D. G. (1989) *J. Magn. Reson.* (in press).

Zarbl, H., Sukumar, S., Arthur, A. V., Martin-Zanca, D., & Barbacid, M. (1985) *Nature 315*, 382–386.